Applied Catalysis B: Environmental 307 (2022) 121167

Contents lists available at ScienceDirect

Applied Catalysis B: Environmental

journal homepage: www.elsevier.com/locate/apcatb

# Facile one-pot synthesis of Ni-based catalysts by cation-anion double hydrolysis method as highly active Ru-free catalysts for green $H_2$ production via $NH_3$ decomposition

Quoc Cuong Do, Youngmin Kim, Thien An Le, Geo Jong Kim, Jeong-Rang Kim, Tae-Wan Kim, You-Jin Lee, Ho-Jeong Chae *

*Chemical & Process Technology Division, Korea Research Institute of Chemical Technology, 141 Gajeong-ro, Yuseong-gu, Daejeon 34114, Republic of Korea*

ARTICLE INFO

*Keywords:*
Ru-free catalysts
Cation-anion double hydrolysis
Ammonia decomposition
Hydrogen production
One-pot synthesis

ABSTRACT

A series of $Ni/Al_1Ce_aO_x$ composites prepared by various synthetic methods, including one-pot anion-cation double hydrolysis (CADH), co-precipitation (CP), CADH followed by wet impregnation (CADH-WI), and CP followed by wet impregnation (CP-WI) were employed as catalysts for ammonia ($NH_3$) decomposition to generate hydrogen. The results revealed that the catalyst prepared by the one-pot CADH method exhibited outstanding catalytic performance (complete $NH_3$ decomposition at around 550 °C) mainly because of significant enhancement in Ni dispersion, Ni reducibility, the quantity of surface oxygen vacancy, and $NH_3$ adsorption affinity. The superior catalytic performance of Ce-containing catalysts over $Ni/Al_2O_3$ catalyst was ascribed to the synergistic effects of NiO reducibility, surface oxygen vacancies, basicity, and Ni-support interaction. The selected catalysts demonstrated excellent stability during 100 h continuous operation, without any obvious decrease in $NH_3$ conversion. Overall, the proposed one-pot CADH method offers great advantages in preparing highly active and stable Ni-based catalysts for $NH_3$ decomposition.

## 1. Introduction

Hydrogen has received significant attention as a clean energy source due to its high gravimetric energy content and zero carbon emission [1]. However, its low volumetric energy density, low boiling point, and handling difficulties (i.e., transport and storage) are major drawbacks for industrial and commercial applications of this gas. These problems can be overcome by using hydrogen carriers, which can be transported easily to the consumption area, and reformed or decomposed to generate hydrogen on-site [2–4]. Among various hydrogen carriers, $NH_3$ has appeared as an excellent candidate due to its low production cost, high volumetric and gravimetric energy density, ease of liquefaction, and clean molecular storage medium; as well, it can be catalytically decomposed into carbon-free hydrogen [4,5]. Nowadays, the catalytic decomposition of $NH_3$ has become a promising approach for hydrogen production, and enormous effort has been devoted to developing a highly efficient catalyst for this reaction. Research has shown that the best catalytic systems for low-temperature $NH_3$ decomposition are currently based on the precious metal ruthenium (Ru); however, the rarity and expense of Ru could hinder its large-scale applications [6,7]. Consequently, the exploration of inexpensive, highly active, and stable catalysts to meet the demand for low-cost catalytic systems has recently attracted great attention. In this respect, nickel (Ni)-based catalysts have been shown as great alternatives for $NH_3$ decomposition because their performances are better than those of any other non-noble metal-based catalysts [8,9].

It is well known that the physicochemical property and performance of Ni-based catalysts are highly dependent on the nature of the support, as well as the synthetic procedures. Regarding the catalyst support material, the $NH_3$ decomposition reaction is generally compatible with supports that have a high surface area, strong alkalinity, high thermal stability, and good electron transferability [7]. Various single metallic oxides (i.e., $Al_2O_3$, $CeO_2$, $La_2O_3$, MgO, $SiO_2$, $TiO_2$, $Y_2O_3$, $ZiO_2$, etc.) have been employed as supports for Ni catalyst in $NH_3$ decomposition, and $Al_2O_3$ has been recognized as one of the most effective supports, mainly due to its great surface area (200 $m^2/g$) and thermal stability [7,10].

* Correspondence to: Chemical & Process Technology Division, Korea Research Institute of Chemical Technology (KRICT),141 Gajeong-ro, Yuseong-gu, Daejeon 34114, South Korea.

*E-mail addresses:* cuongdo@krict.re.kr (Q.C. Do), ykim@krict.re.kr (Y. Kim), thienan@krict.re.kr (T.A. Le), kujong@krict.re.kr (G.J. Kim), jrkim@krict.re.kr (J.-R. Kim), twkim@krict.re.kr (T.-W. Kim), eugene@krict.re.kr (Y.-J. Lee), hjchae@krict.re.kr (H.-J. Chae).

https://doi.org/10.1016/j.apcatb.2022.121167
Received 4 October 2021; Received in revised form 26 January 2022; Accepted 30 January 2022
Available online 3 February 2022

$Al_2O_3$ is also an attractive choice for economical hydrogen production systems. Besides this, the modification of $Ni/Al_2O_3$ catalyst by introducing an appropriate amount of promoter is an interesting approach to further enhance its catalytic performance. The addition of rare earth elements has proved able to speed up the rate-limiting steps in $NH_3$ decomposition reaction [11]. Cerium (Ce), an abundant rare earth metal, its oxide has several outstanding features, especially, the formation of a large number of and high mobility of surface oxygen vacancies under reducing atmosphere due to the existence of reversible valence couple ($Ce^{4+}/Ce^{3+}$); this makes Ce an excellent support/promoter agent for a wide range of catalysts in $NH_3$ decomposition reaction [12–14]. It was reported that the combination of Ce and $Ni/Al_2O_3$ catalyst could enhance both the catalytic activity and stability for $NH_3$ decomposition [15,16]. However, the promotional effects of Ce addition and the method of doping Ce into the $Al_2O_3$ framework for Ni catalyst have not been sufficiently explored.

Various synthetic techniques have been applied for $Ni/Al_2O_3$ catalyst development, including deposition-precipitation (DP) [17], wet impregnation (WI) [9], co-precipitation (CP) [18], and solution combustion (SC) [19]. Catalysts prepared by DP or WI methods generally suffer from thermal sintering of Ni species, and catalytic activity is highly dependent on the nature of support [7]. The CP method has a certain advantage in terms of thermal stability, but the use of basic precipitation agents might raise concerns about environmental pollution. The SC method is an effective technique for producing uniform and highly-dispersed catalysts, but the use of organic fuels, such as urea, alcohols, glycine, etc., can lead to unavoidable waste of reagents [20]. Therefore, the development of a new synthetic technique that meets the above requirements is needed for industrial applications. In this context, a facile one-pot cation-anion double hydrolysis (CADH) method, formerly applied for the preparation of thermally stable mesoporous $\gamma$-$Al_2O_3$, has shown several outstanding advantages such as the use of cheaper $Al_2O_3$ sources, simple synthesis procedure, faster hydrolysis of the $Al_2O_3$ precursor, high surface area and basic surface nature of derived $Al_2O_3$ [21,22]. To the best of our knowledge, the catalyst prepared by the CADH method for $NH_3$ decomposition has not been reported in the literature.

Herein, we integrated Ce and Ni with $Al_2O_3$ using the facile one-pot CADH method for the preparation of Ce promoted $Ni/Al_2O_3$ catalyst, aiming at high catalytic performance for $NH_3$ decomposition; we also hope to clarify the role of Ce in the derived catalysts. To accomplish these objectives, we initially prepared a series of $10Ni/Al_1Ce_{0.05}O_x$ catalysts by various synthetic methods and evaluated their catalytic activities for the reaction. The best synthesis method was then applied for the preparation of catalysts with various Ce/Al molar ratios to achieve a better understanding of the promotional effects of Ce in this reaction. Furthermore, the synthetic procedure and reaction conditions were experimentally optimized.

## 2. Experimental

### 2.1. Catalyst preparation

A series of Ni-Ce-Al catalysts with various Ni weight percentages (10 – 60 wt%) and Ce/Al molar ratios (0 – 0.10) were synthesized via a facile one-pot CADH method [20] with some modifications in the synthetic procedure. In a typical process, designated amounts of Ni, Ce nitrate precursors ($Ni(NO_3)_2.6H_2O$, $Ce(NO_3)_3.6H_2O$), and aluminum precursor ($NaAlO_2$) were separately dissolved in deionized water (50 mL each). The Ni, Ce nitrate precursors mixed solution was then added dropwise into the aluminum precursor solution under stirring, and the pH of the homogeneously mixed solution was controlled in the range of 8.0–12.0 using 1.0 M $HNO_3$ and/or 1.0 M $NH_4OH$ solution. The hydrolysis and aging processes were carried out for 20 h under vigorous stirring at 25 $^oC$. The resulting precipitate was obtained by filtration, followed by thorough washing with deionized water and ethanol. The samples were dried at 100 °C overnight, then ground, and subsequently calcined in a muffle furnace (Vulcan 3–550, Neytech, USA) at 600 °C for 5 h with a ramping rate of 3 °C/min under air atmosphere. The obtained catalysts were denoted $ANi/Al_1Ce_aO_x$, in which the prefix $A$ represents Ni weight percentage (wt%) contained in the samples, and $a$ is the molar ratio of Ce to Al. Our preliminary study has determined the optimum pH condition of the above Ni, Ce, Al mixed solution (pH 10.0), at which the obtained catalyst exhibited the highest performance for $NH_3$ decomposition (Fig. S1). Consequently, the pH condition of the mixed solution will be controlled at 10.0 in this study.

To compare this method with various other preparation methods, $10Ni/Al_1Ce_{0.05}Ox$ catalysts were prepared by co-precipitation (CP), CADH followed by wet impregnation (CADH-WI), and CP followed by wet impregnation (CP-WI) methods. For the CP method, Ni $(NO_3)_2.6H_2O$, $Al(NO_3)_3.9H_2O$, and $Ce(NO_3)_3.6H_2O$ with appropriate ratios were dissolved in 100 mL deionized water, followed by dropwise addition of $NH_4OH$ solution (1.0 M) under vigorous stirring. The precipitate was aged overnight at room temperature, then collected by filtration, and thoroughly washed with deionized water and ethanol. The samples were dried in an air oven at 100 °C overnight, then ground and calcined under the same conditions mentioned above. For the CADH-WI and CP-WI methods, the $Al_1Ce_{0.05}O_x$ supports were first prepared by CADH and CP methods, respectively, under conditions otherwise identical to the preparation of the corresponding catalysts without the presence of Ni precursor. The obtained $Al_1Ce_{0.05}O_x$ supports were then dispersed in 100 mL deionized water under vigorous stirring, followed by the addition of a suitable amount of $Ni(NO_3)_2.6H_2O$. The mixtures were stirred at 60 $^oC$ for 5 h and, subsequently, the solvent was removed by rotary evaporation. The impregnated samples were then dried in an air oven at 100 $^oC$ overnight, ground, and calcined in the air atmosphere at 600 °C for 5 h with a ramping rate of 3 °C/min.

### 2.2. Catalyst characterization

Powder X-ray diffraction (XRD) patterns of the catalysts were obtained using a high-resolution powder X-ray diffractometer (SmartLab, Rigaku, Japan). The measurement was operated at a scanning speed of $5^o$/min in the $2\theta$ range of 20 – $80^o$.

X-ray photoelectron spectra (XPS) were recorded on an X-ray photoelectron spectroscope (Axis-Supra, Kratos, UK). All obtained spectra were corrected using the C1s signal located at a binding energy of 284.8 eV.

Transmission electron microscopy (TEM) images were taken on a transmission electron microscope equipped with an energy dispersive X-ray spectrometer (FEI Tecnai G2–20 S-Twin, FEI Technologies Inc., USA).

The specific surface area ($S_{BET}$) of the calcined catalysts was characterized with nitrogen adsorption/desorption at – 196 $^oC$ using a surface area and porosity analyzer (Tristar 3000, Micromeritics Instrument Co., USA) according to the Brunauer–Emmett–Teller method, all the samples were degassed in a vacuum atmosphere at 200 $^oC$ for 4 h before the measurements. Inductively coupled plasma optical emission spectroscopy (Agilent ICP-OES 720, Agilent, USA) was employed to determine the elemental composition of the catalysts.

$H_2$ chemisorption was conducted using an accelerated surface area and porosimetry system (ASAP 2020, Micromeritics Instrument Corp., USA). Before the analysis, the calcined catalyst samples were reduced in $H_2$ flow at 600 $^oC$ for 2 h, then cooled to room temperature in He flow. The analysis was performed at room temperature with pure $H_2$ flowing at 50 mL/min. The Ni dispersion ($D_{Ni}$) and Ni surface area ($S_{Ni}$) were calculated by assuming a Ni/H adsorption stoichiometry factor of 2 and a Ni atomic cross-sectional area of 0.0649 $nm^2$.

Hydrogen-temperature-programmed reduction ($H_2$-TPR) was performed to evaluate the reducibility of catalysts using a chemisorption analyzer (Belcat-B, MicrotracBEL Corp., Japan). The calcined samples were pretreated at 300 $^oC$ with He gas flowing at 50 mL/min, then

cooled to 40 °C. The pretreated catalyst was exposed to 10% $H_2$/Ar flowing at 50 mL/min, and the $H_2$-TPR profiles were recorded while the temperature was increased to 1000 °C at a heating rate of 10 °C/min.

Temperature-programmed desorption of $CO_2$ ($CO_2$-TPD) was performed on a chemisorption analyzer (AutoChem II 2920, Micromeritics Instrument Corp., USA) equipped with a quadrupole mass spectrometer (Cirrus 2, MKS Instruments Inc., USA). The catalyst was pretreated with $H_2$ at 600 °C for 2 h, then purged with He gas at 50 mL/min to remove the adsorbed $H_2$. After cooling to 50 °C, the catalyst was exposed to $CO_2$ flow at 50 mL/min for 1 h, and then He gas was supplied (50 mL/min) to eliminate the residual $CO_2$ gas. Desorption profiles of $CO_2$ ($m/z = 44$) were monitored during the increase of temperature to 600 °C at an increment rate of 10 °C/min.

Temperature-programmed desorption of $NH_3$ ($NH_3$-TPD) was carried out using the chemisorption analyzer equipped with the quadrupole mass spectrometer. The samples were pretreated with $H_2$ at 600 °C for 2 h, then purged with He gas to remove $H_2$ adsorbed during the reduction. After cooling to 50 °C, 5% $NH_3$/He was introduced to the reactor at a flow rate of 100 mL/min for 1 h; then purged with He gas. Desorption profiles of $NH_3$ ($m/z = 17$), $N_2$ ($m/z = 28$), and $H_2$ ($m/z = 2$) were obtained during the increase of temperature to 600 °C at an increment rate of 10 °C/min.

$NH_3$ temperature-programmed surface reaction ($NH_3$-TPSR) analysis was performed on the chemisorption analyzer to clarify the desorption behavior of the reactant and product species during the reaction. Before the measurement, the samples were reduced in the $H_2$ atmosphere at 600 °C for 2 h. After cooling to 50 °C in He flow, 5% $NH_3$/He was continuously supplied at a rate of 100 mL/min. $NH_3$-TPSR was performed by raising the temperature to 800 °C with a heating rate of 10 °C/min. Residual $NH_3$ ($m/z = 17$), recombinative $H_2$ ($m/z = 2$) and $N_2$ ($m/z = 28$) desorption were analyzed by the mass spectrometer.

In-situ diffuse reflectance infrared spectroscopy (DRIFTS) study of species adsorbed on the catalysts when contact with $NH_3$ during the heating process was conducted using a Nicolet iS10 FTIR spectrometer (Thermo Fisher Scientific Inc., USA) equipped with a diffuse reflectance accessory. Catalysts were loaded into the DRIFTS cell and pretreated under $H_2$ atmosphere at 500 °C for 2 h, then allowed to cool to 50 °C in He flow (100 mL/min). The samples were continuously exposed to 5% $NH_3$/He at a rate of 100 mL/min and temperatures of 50, 100, 200, 300, 400, and 500 °C. Spectra of catalysts at each temperature were recorded via auto scanning at a resolution of 4 $cm^{-1}$ with 100 accumulated scans.

X-ray absorption fine structure (XAFS) recorded for the Ni K-edge were obtained with the 7D beamline system at the Pohang Accelerator Laboratory (PAL), which is equipped with a Si (111) double crystal monochromator (PLS-II, 3.0 GeV, Republic of Korea). Ni metal foil and NiO were used as reference materials.

### 2.3. Catalytic activity tests

The $NH_3$ decomposition over the prepared catalysts was evaluated at atmospheric pressure in a quartz fixed-bed continuous-flow straight tube reactor equipped with a thermocouple. In a typical reaction, 0.1 g of catalyst sample was loaded on a quartz wool layer inside the reactor, followed by heating to 600 °C at 4 °C/min under a continuous flow of pure $H_2$ (30 mL/min) and holding for 2 h thereafter. The sample was then allowed to cool to 300 °C in an argon atmosphere (10 mL/min). After that, pure gaseous $NH_3$ (10 mL/min), corresponding to a weight hourly space velocity (WHSV) of 6000 mL/$g_{cat.}$/h, was introduced into the reactor. The catalytic activity was evaluated at various temperatures ranging from 300 °C to 600 °C with steps of 50 °C (60 min at each temperature). An online gas chromatography (YL6500GC, YL Instrument Co., Korea) equipped with a thermal conductivity detector (TCD), and Porapak-N and Molesieve 13X columns, were used to monitor the concentration of outlet gases. The $NH_3$ conversion $X_{NH_3}$(%) was calculated by taking into account the gas phase volume changes under constant reaction temperature and the total pressure in the plug-flow system, as expressed in the Eq. (1) [23]. The hydrogen formation rate $r_{H_2}$ (mmol/$g_{cat.}$/min) was calculated according to Eq. (2), and the apparent activation energy $E_{app}$ (kJ/mol) was calculated using the Arrhenius Eq. (3).

$$X_{NH_3} = \frac{[NH_3]_{in} - [NH_3]_{out}}{[NH_3]_{in} + [NH_3]_{out}} \times 100 \quad (1)$$

$$r_{H_2} = \frac{\frac{V_{NH_3}}{22.4}.X_{NH_3}.1.5}{m_{cat.}} \quad (2)$$

$$k = k_0 e^{-E_{app}/RT} \quad (3)$$

where $[NH_3]_{in}$, and $[NH_3]_{out}$ are the $NH_3$ concentrations in the inlet and outlet gases, respectively. $V_{NH_3}$ is the $NH_3$ flow rate (mL/min), $m_{cat.}$ is the mass of catalyst (g), k is the reaction constant (mol/$g_{cat.}$/s), $k_0$ is the frequency factor (mol/$g_{cat.}$/s), R is the universal gas constant (kJ/mol/K), and T is the absolute temperature (K).

## 3. Results and discussion

### 3.1. General property of catalysts

The Ni content, and the molar ratio between Al and Ce of the prepared catalysts, were verified by ICP-OES analysis, and the corresponded data are presented in Tables 1 and 2. All data closely matched the theoretical calculations, indicating the successful preparation of the targeted materials. The XRD patterns of the calcined and reduced (reduction at 600 °C in $H_2$ atmosphere) catalysts shown in Fig. S2 indicate the formation of $CeO_2$, NiO, $NiAl_2O_4$, γ-$Al_2O_3$, and Ni phases in the structures. However, it should be noted that the diffraction peaks of $NiAl_2O_4$ spinel and NiO can be overlapped by those of γ-$Al_2O_3$. Besides, the metallic Ni peaks were not observed in the Ce-promoted catalysts prepared by the CADH method (Figs. S2b and d). This observation suggested that the Ni phase in these samples might be a more amorphous structure with a smaller Ni size than the non-promoted catalysts and the other catalysts prepared by the non-CADH process. The overall morphology and elemental composition of the reduced catalysts prepared by various methods can be seen in Fig. 1 and S3. TEM images of the catalysts reveal that the Ni size (dark spots) is about 3.9–5.0 nm, and Ni is well dispersed throughout the support matrix. Elemental distribution mapping confirmed the homogeneous distribution of Ni, Al, and Ce atoms in the prepared catalysts. $N_2$ adsorption/desorption isotherms of the samples were typical type IV isotherms (Fig. 2a and S4a), confirming the mesoporous structure of the catalysts. Besides this, the pore size distribution (PSD) profile exhibited a bimodal shape for all the Ce-containing catalysts (Fig. 2b and S4b). The local structure and electronic nature of the Ni phases were explored with XAFS characterization. The normalized Ni K-edge X-ray absorption near-edge structure (XANES) spectra and $k^3$-weighted Fourier transform of extended X-ray absorption fine structure (EXAFS) spectra for the reduced catalysts and reference materials (Ni foil and NiO) are presented in Fig. 3 and S5, respectively. The normalized Ni-K-edge XANES spectra showed that the absorption edge position and whiteline intensity of all the prepared catalysts (Fig. 3) are between those of Ni foil and the NiO bulk structure, suggesting the features of both metallic Ni and NiO in the catalysts. The results were also confirmed by the linear combination fit (LCF) of the corresponding Ni K edge XANES spectra of the catalysts (Fig. S6). This indicates that the Ni species in the catalysts were not completely reduced during the reduction process [20], and/or were re-oxidized due to possible exposure to air during sample processing. These results are in accordance with the XPS results, in which both $Ni^{2+}$ and $Ni^0$ were detected (Table 1). In the EXAFS spectra (Fig. S5), the peaks of the Ni-O bonds (1.5–1.7 Å) and Ni-Ni bonds in NiO (2.7 – 2.8 Å) are comparable for all investigated catalysts; however, the peak corresponding to Ni-Ni bonds (2.1–2.2 Å) in Ni metal was not observed for the Ce-containing

**Table 1**
Physicochemical properties of the reduced $Ni/Al_1Ce_{0.05}O_x$ catalysts prepared by various methods.

| Method | Ni (wt%)[a] | Ce/Al (mole)[a] | $D_{Ni}$ (%)[b] | $S_{Ni}$ ($m^2/g$)[b] | $S_{BET}$ ($m^2/g$) | $H_2$ consumption (mmol/g)[c] | $\%Ni^0/(Ni^0+Ni^{2+})$[d] | $\%Ce^{3+}/(Ce^{3+}+Ce^{4+})$[d] |
|---|---|---|---|---|---|---|---|---|
| CADH | 9.6 | 0.05 | 5.72 | 4.25 | 274 | 14.25 | 8.16 | 53.13 (40.50) |
| CADH-WI | 9.3 | 0.05 | 1.87 | 1.32 | 209 | 5.87 | 6.82 | 46.67 (34.63) |
| CP | 9.7 | 0.05 | 1.36 | 0.88 | 188 | 4.70 | 4.73 | 45.30 (30.22) |
| CP-WI | 9.5 | 0.05 | 2.97 | 2.12 | 221 | 6.64 | 7.38 | 49.17 (34.12) |

[a] Determined by ICP-OES analysis.
[b] Measured by $H_2$ chemisorption analysis.
[c] Calculated based on $H_2$-TPR profile for the reduction from 40 °C to 600 °C.
[d] Obtained from XPS spectra of the reduced catalysts, the numbers in the parentheses are represented for the calcined samples.

**Table 2**
Physicochemical properties of the reduced catalysts prepared by CADH methods.

| Samples | Ni (wt%)[a] | Ce/Al (mole)[a] | $D_{Ni}$ (%)[b] | $S_{Ni}$ ($m^2/g$)[b] | $S_{BET}$ ($m^2/g$) | $H_2$ consumption (mmol/g)[c] | $\%Ni^0/(Ni^0+Ni^{2+})$[d] | $\%Ce^{3+}/(Ce^{3+}+Ce^{4+})$[d] |
|---|---|---|---|---|---|---|---|---|
| $10Ni/Al_2O_3$ | 9.6 | 0.00 | 7.01 | 5.21 | 261 | 8.12 | 12.96 | – |
| $10Ni/Al_1Ce_{0.01}O_x$ | 9.9 | 0.01 | 8.38 | 6.49 | 309 | 6.87 | 10.41 | 43.84 |
| $10Ni/Al_1Ce_{0.02}O_x$ | 9.9 | 0.02 | 7.24 | 5.54 | 293 | 9.46 | 9.73 | 45.27 |
| $10Ni/Al_1Ce_{0.05}O_x$ | 9.6 | 0.05 | 5.72 | 4.25 | 274 | 14.25 | 8.16 | 53.13 |
| $10Ni/Al_1Ce_{0.10}O_x$ | 9.4 | 0.11 | 5.41 | 3.90 | 273 | 19.84 | 4.92 | 43.66 |
| $20Ni/Al_1Ce_{0.05}O_x$ | 19.3 | 0.05 | 7.20 | 10.25 | 245 | 23.18 | 11.24 | 59.39 |
| $40Ni/Al_1Ce_{0.05}O_x$ | 38.4 | 0.05 | 7.97 | 20.39 | 239 | 38.40 | 19.39 | 71.00 |
| $60Ni/Al_1Ce_{0.05}O_x$ | 52.4 | 0.05 | 4.71 | 16.45 | 193 | 42.25 | 16.95 | 50.91 |

[a] Determined by ICP-OES analysis.
[b] Measured by $H_2$ chemisorption analysis.
[c] Calculated based on $H_2$-TPR profile for the reduction from 40 °C to 600 °C.
[d] Obtained from XPS spectra of the reduced catalysts.

catalysts prepared by CADH method. Besides this, the peaks of Ni-Ni (NiO) for all Ni-supported catalysts appeared with low intensity compared to that for NiO, signifying that this location is mixed with Ni-Ni and Ni-M (M = Al, Ce) [24,25]. The effects of synthetic methods, the promotional effects of Ce, and the influence of synthetic and operating conditions on $NH_3$ decomposition are thoroughly discussed based on the distinct properties of each specific catalyst in the following sections.

### 3.2. One-pot CADH method enhances $NH_3$ decomposition

Fig. 4a shows the performance of $NH_3$ decomposition over $10Ni/Al_1Ce_{0.05}O_x$ catalysts prepared by various methods at a WHSV of 6000 mL/$g_{cat.}$/h. The $NH_3$ conversion rapidly increased with the increase of reaction temperature, which is in accordance with the endothermic nature of the $NH_3$ decomposition reaction. However, the catalytic activity varied significantly with different preparation methods. The one-pot CADH method provided the catalyst with the highest $NH_3$ conversion and the lowest apparent activation energy (74.72 kJ/mol) (Table S2). The differences in the obtained apparent activation energies could be due to the differences in the state of surface $Ni^0$ fraction [26] and/or the kind of active Ni facet [27] in the catalysts. The one-pot CADH-derived catalyst can complete the reaction at 550 °C with the $H_2$ formation rate of 6.70 mmol/$g_{cat.}$/min. The catalytic performance was observed to decrease in the order of catalysts prepared by CADH, CP-WI, CADH-WI, and CP methods (Fig. 4a and Table S2). These results were further confirmed by $NH_3$-TPSR-MS measurement, in which the profiles of reactant and product species ($N_2$ and $H_2$) were in line with the activity tests (Fig. 5a). On the other hand, the $NH_3$-TPD-MS results showed significant differences in the desorption behavior of $NH_3$, $N_2$, and $H_2$ over these catalysts (Fig. 5b). Although $NH_3$ desorption proceeded from 80 °C to around 500 °C for all catalysts, the CADH-derived catalyst exhibited the largest $NH_3$ desorption peak, along with the largest $H_2$ and $N_2$ desorption peaks. This indicated that the CADH-derived catalyst had a better $NH_3$ adsorption capacity than those of other catalysts. Meanwhile, except for that of the CADH-derived catalyst, the $NH_3$ desorption peak of the CP-derived catalyst was larger than those of other catalysts, and its corresponding $H_2$ and $N_2$ desorption peaks were smaller and appeared at higher temperatures regions (especially for the $H_2$ desorption peak). This implies that the $NH_3$ adsorbed on this catalyst was slightly decomposed, and the recombinative $N_2$ and $H_2$ desorption proceeded less readily than they did over other catalysts.

Because metallic Ni is the active phase in this reaction [6], the performances of these $10Ni/Al_1Ce_{0.05}O_x$ catalysts are considerably related to Ni properties including size, dispersion, and surface area. Indeed, the increase in Ni size leads to a decrease in the catalytic activity, which is consistent with the trend of Ni size observed in the TEM results (Fig. 1). As can be seen in Table 1, the sample prepared by the CADH method possesses the highest Ni dispersion (5.72%) and the largest Ni surface area (4.25 $m^2/g$), which exhibited the best catalytic performance. These data are consistent with the $H_2$-TPR profiles of the corresponding catalysts (Fig. 6a), in which the $H_2$ consumption peaks of highly active catalysts are more pronounced at lower temperature regions. Evidently, the CADH derived catalyst showed more obvious peaks in the low-temperature region (< 400 °C); these are related to the greater quantity of reducible oxygen species in the NiO-$CeO_2$ solid solutions [15]. Besides this, $H_2$ consumption during the reduction from 40 to 600 °C of the $10Ni/Al_1Ce_{0.05}O_x$ catalysts (Table 1) exhibited a good correlation with overall catalytic activity: the highest value was observed for the catalyst prepared by the CADH method (14.25 mmol/g). Noticeably lower values were recorded for other catalysts prepared by CP-WI, CADH-WI, and CP methods: 6.64, 5.87, and 4.70 mmol/g, respectively. The lower of these values suggests that the reduction of NiO in the catalysts prepared by CP-WI, CADH-WI, and CP methods below 600 °C is more difficult, implying that the interactions of Ni species inside the structures of these catalysts are much stronger than in the CADH-derived catalyst. This is also supported by the shifting of major $H_2$ consumption peaks to higher temperature regions (750–900 °C) in the $H_2$-TPR profiles, implying that there was more stable $NiAl_2O_4$ spinel formation in catalysts prepared by CP-WI, CADH-WI, and CP methods, which is in accordance with the XRD results shown in Fig. S2.

The surface chemical states of Ni and Ce in the calcined and reduced

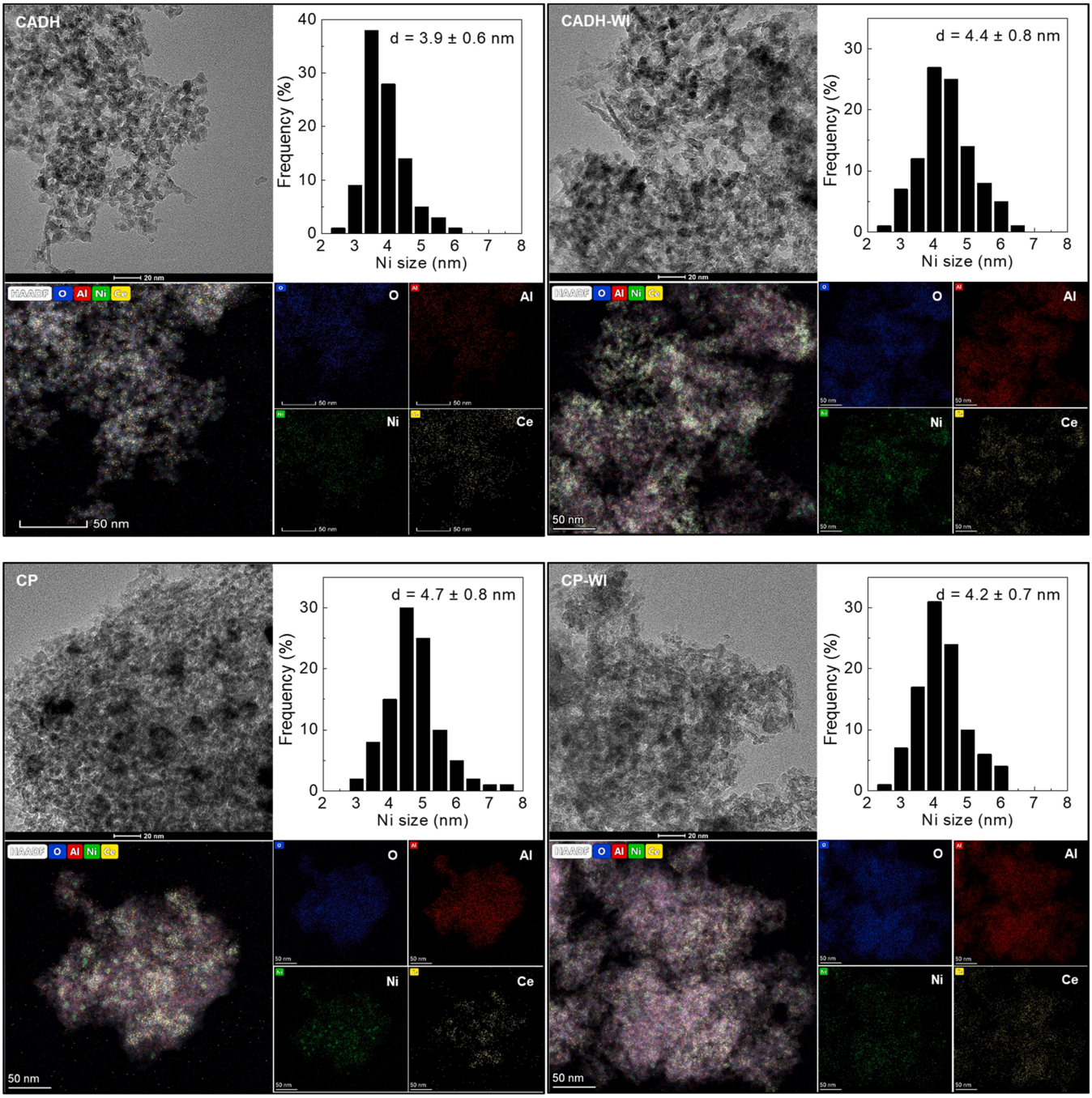


**Fig. 1.** Typical TEM images, EDS elemental mapping images, and Ni size distribution of the reduced $10Ni/Al_1Ce_{0.05}O_x$ catalysts prepared by various methods.

catalysts prepared by various synthetic methods can be observed in their corresponding XPS spectra (Fig. 7 and S7). The spectra of Ni 2p (Fig. 7a) for all reduced samples show the co-existence of different Ni species, indicating an incomplete transformation of nickel oxide into the metallic state after the reduction at 600 °C. Evidently, the peaks at binding energy around 852.7 eV are represented for surface $Ni^0$ [28] that are formed after the reduction process, as compared to the corresponding spectra of the calcined catalysts (Fig. S7). The peaks at around 856.0 eV are assigned to the $Ni^{2+}$ due to their interactions with aluminum oxide and/or cerium oxides [29,30]. The peaks at around 861.4 eV can be associated with the shake-up satellite peak of $Ni^{2+}$ [1]. The surface $Ni^0$ fraction, $Ni^0/(Ni^0 + Ni^{2+})$, represents the quantity of $Ni^0$ formation on the catalyst surface after the reduction, and the highest value (8.16%) was observed for the catalyst prepared by the one-pot CADH method (Table 1). The results are consistent with the above $H_2$-TPR discussion, confirming that the CADH-derived catalysts can be reduced easier than other catalysts under the same reduction conditions. The high reducibility of CADH-derived catalyst is also supported by the XPS spectra of the calcined catalysts (Fig. S7), in which the $Ni^{2+}$ peaks shift to lower binding energies compared to those of other catalysts, resulting in a weaker interaction with the supports [30]. Interestingly, the bulk $Ni^0$ fraction of catalysts (Table S1) does not seem to affect the catalytic activity because the CADH-derived catalyst has a smaller bulk $Ni^0$ fraction (15.30%) than the less active CP-WI derived catalyst (43.30%). Therefore, the surface $Ni^0$ fraction (active sites) of the catalyst is more strongly determined the catalytic performance in this reaction. On the other hand, the deconvolution of the Ce 3d XPS spectra of these catalysts suggests that Ce existed in both $Ce^{3+}$ and $Ce^{4+}$ states (Fig. 7b). The $Ce^{3+}$

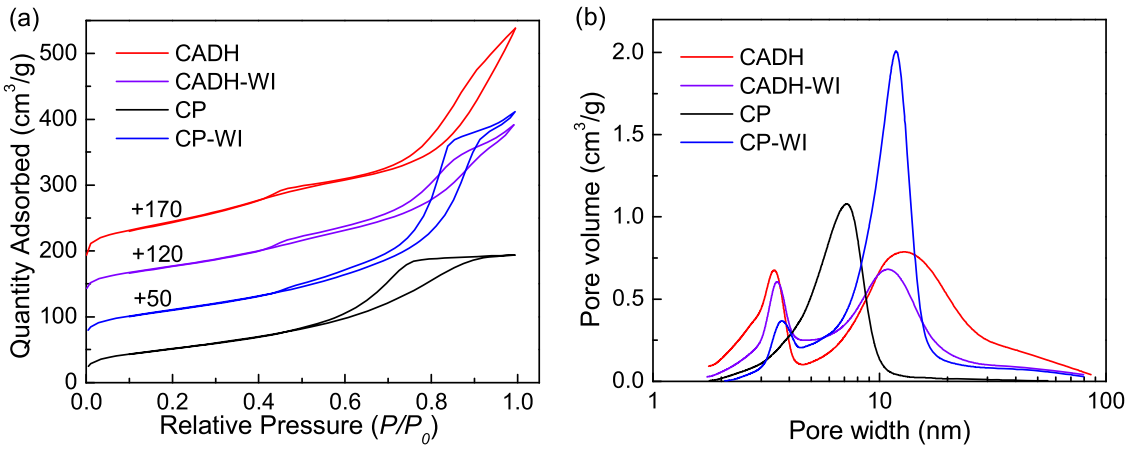


**Fig. 2.** $N_2$ adsorption/desorption isotherms (a) and pore-size distribution (b) of the calcined $10Ni/Al_1Ce_{0.05}O_x$ catalysts prepared by various methods.

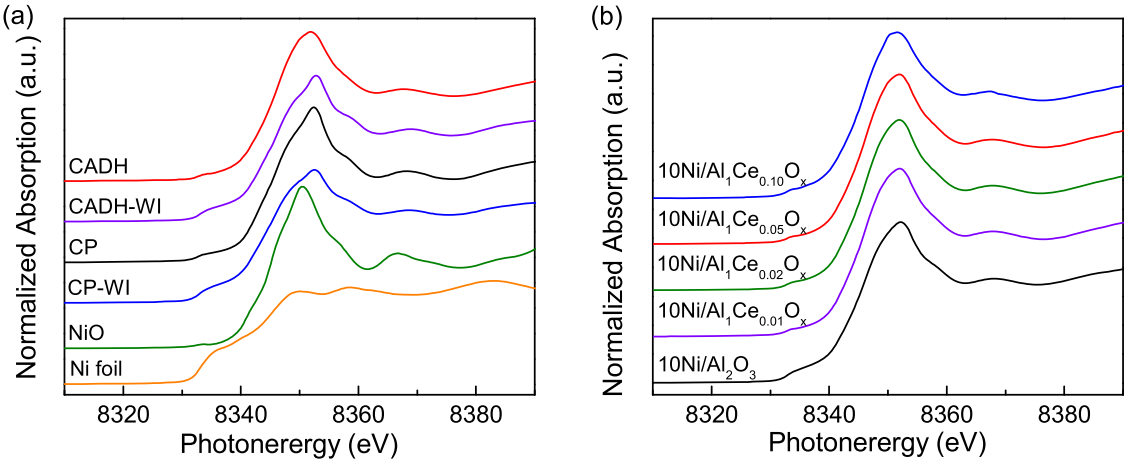


**Fig. 3.** Normalized Ni K-edge XANES spectra for Ni foil, NiO, and the reduced $10Ni/Al_1Ce_{0.05}O_x$ catalysts prepared by various methods (a) and those for the reduced catalysts with different Ce/Al molar ratios (b).

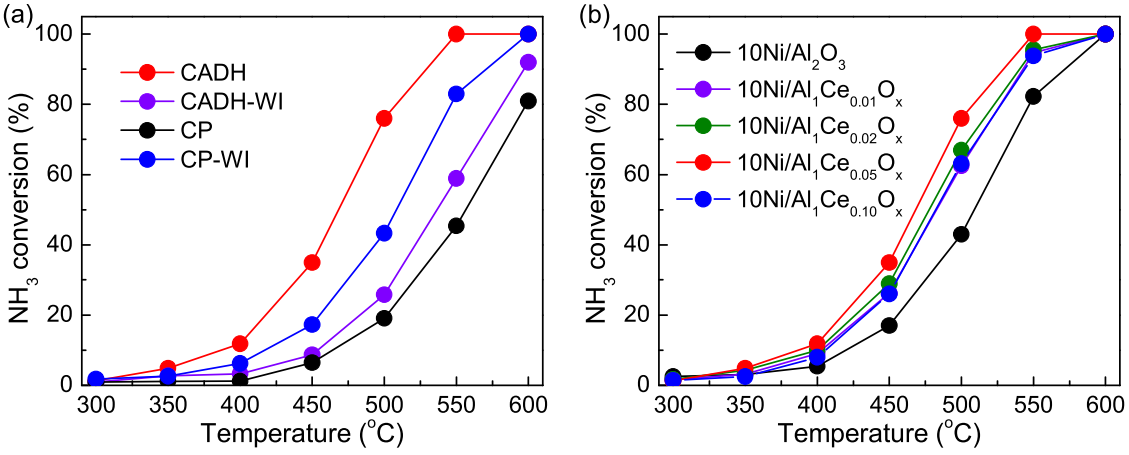


**Fig. 4.** Catalytic activity for $NH_3$ decomposition over $10Ni/Al_1Ce_{0.05}O_x$ catalysts prepared by various methods (a) and those over catalysts with different Ce/Al molar ratios prepared by CADH method (b).

species are represented by four peaks located at binding energies around 879.9, 885.5, 898.3, and 904.0 eV, while $Ce^{4+}$ species are represented by six peaks corresponding to binding energies at around 882.2, 888.8, 896.6, 900.9, 907.3, and 916.6 eV. The surface ratio of $Ce^{3+}$ to total Ce, including $Ce^{3+}$ and $Ce^{4+}$, is summarized in Table 1. The increase of the surface $Ce^{3+}$ ratio in the reduced catalysts compared to those of corresponding calcined catalysts signifies the formation of oxygen vacancies [31]. To take the different surface $Ce^{3+}$ proportions into account, the reduced catalyst prepared by the one-pot CADH method exhibited the highest value (Table 1), indicating the presence of the highest quantity

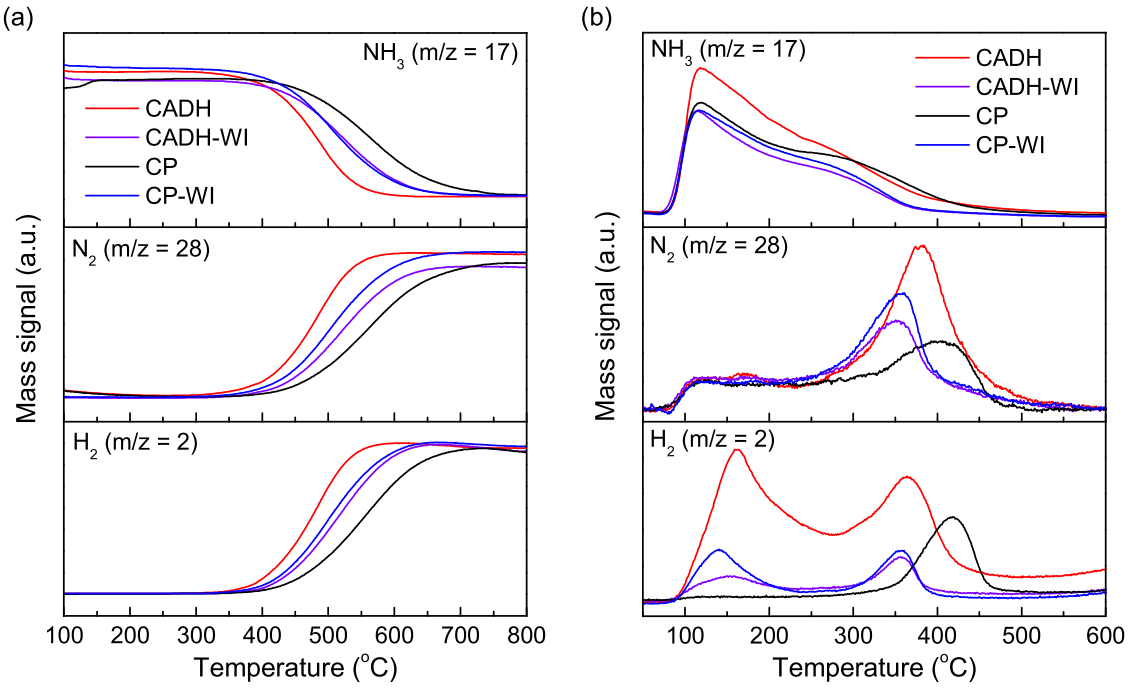


**Fig. 5.** $NH_3$-TPSR-MS (a) and $NH_3$-TPD-MS (b) profiles of $10Ni/Al_1Ce_{0.05}O_x$ catalysts prepared by various methods.

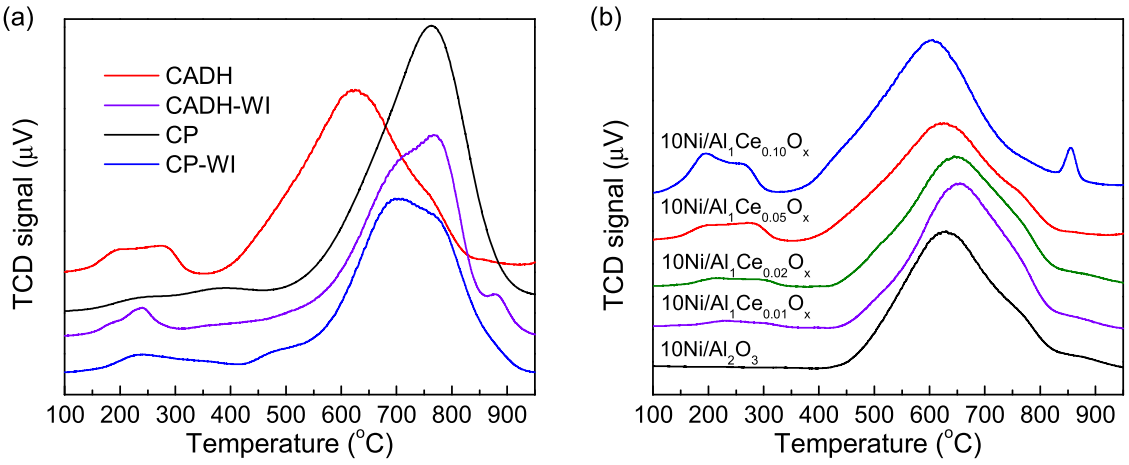


**Fig. 6.** $H_2$-TPR profiles of $10Ni/Al_1Ce_{0.05}O_x$ catalysts prepared by various methods (a) and those of catalysts with different Ce/Al molar ratios prepared by CADH method (b).

of surface oxygen vacancy, which can serve as electron traps and thereby accelerate the catalytic activity [32].

Regarding the textural properties, compared to other methods the one-pot CADH method provided a more porous catalyst, which can be observed in the pore structures summarized in Table 1 and Fig. 2. The largest value of BET surface area was recorded for the catalyst prepared by the one-pot CADH method (274 $m^2/g$), followed by those prepared by CP-WI (221 $m^2/g$), CADH-WI (209 $m^2/g$), and CP (188 $m^2/g$) methods. Besides this, the synthetic procedure significantly affects the pore structure of the catalysts, which can be seen from the changes in the shape of the hysteresis loop in the $N_2$ adsorption/desorption isotherms (Fig. 2a). As illustrated in Fig. 2b, the CP-derived catalyst showed a relatively narrow PSD with monomodal PSD centering at around 7.0 nm, while all the other catalysts exhibited bimodal PSD shapes, and the PSD became wider for the one-pot CADH-derived catalyst centering at around 3.5 nm and 14.0 nm. The catalyst with a bimodal PSD structure may be useful in $NH_3$ decomposition because it contains both macropores and mesopores; macropores can result in a high gas diffusion rate, while mesopores improve catalytic [33,34]. Furthermore, the one-pot CADH method produced a smaller size of $CeO_2$ than those produced by other methods, which can be verified by the intensity of the XRD diffraction peaks corresponding to the $CeO_2$ phase, as shown in Fig. S2. Briefly, it can be said that higher BET surface area, bimodal shape and wider PSD of catalyst, and smaller crystallized size of promoter facilitate adsorption and diffusion of $NH_3$ at the surface of catalysts, enhancing their performance for $NH_3$ decomposition.

In summary, compared to the other investigated methods, the one-pot CADH method offers significant advantages for the production of catalysts, including better Ni dispersion, larger Ni surface area, higher Ni reducibility, higher amount of surface oxygen vacancy, and better $NH_3$ adsorption affinity. These properties are beneficial for the catalytic $NH_3$ decomposition reaction so that the outstanding performance of the CADH-derived catalyst is now understandable.

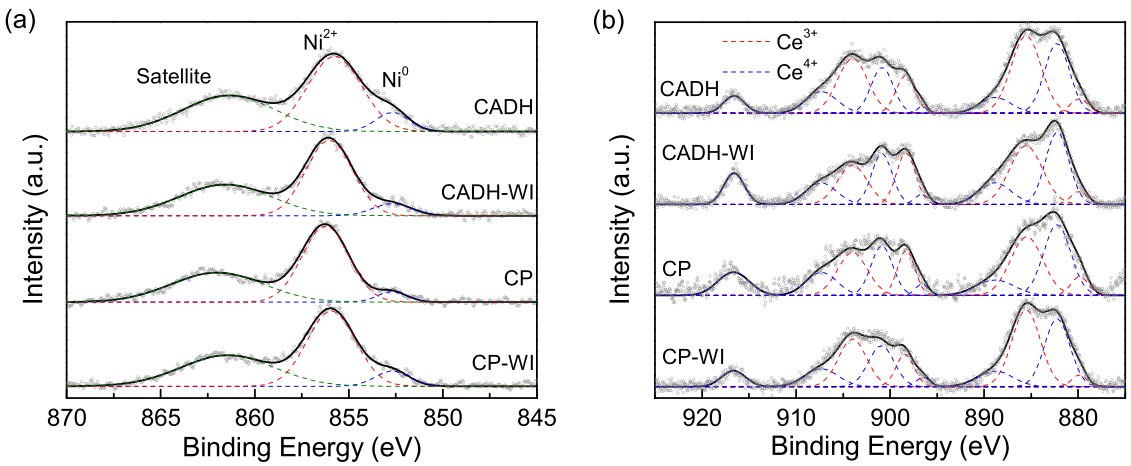


**Fig. 7.** XPS Ni 2p (a) and Ce 3d (b) spectra of the reduced 10Ni/$Al_1Ce_{0.05}O_x$ catalysts prepared by various methods.

### 3.3. Promotional effects of Ce

Fig. 4b shows the performance of 10Ni/$Al_1Ce_aO_x$ catalysts with different Ce/Al molar ratios for $NH_3$ decomposition at a WHSV of 6000 mL/$g_{cat.}$/h. The presence of Ce in the catalysts induced superior catalytic performance compared to that of $Al_2O_3$ supported Ni catalyst. The $NH_3$ conversion increased from 42.97% to 76.03% at 500 °C with the increase of Ce/Al molar ratio to 0.05; the $NH_3$ conversion then decreased with further increasing of this ratio. The results suggested that the presence of a suitable amount of Ce can maximize the catalytic activity of the catalysts.

It has been reported that too much amount of promoter generally decreases the catalytic activity due to coverage of active sites [15,35]. Obviously, the $H_2$-chemisorption results (Table 2) indicate that a small amount of Ce addition (Ce/Al = 0.01) can enhance the Ni dispersion and Ni surface area, but these parameters progressively decreased with greater amounts of Ce addition due to blockage of Ni particles. It was interesting to note that the 10Ni/$Al_1Ce_{0.01}O_x$ catalyst that possessed the highest Ni dispersion (8.38%) and the largest Ni surface area (6.49 $m^2$/g) did not provide the best catalytic activity for $NH_3$ decomposition. These observations suggest that the dispersion and surface area of the active phase are important but are not the only factors controlling the catalytic performance in this reaction.

To allow us to dig deeper into this hypothesis, the $H_2$-TPR profiles of these calcined catalysts are recorded and presented in Fig. 6b. Some small peaks appeared below 400 °C and were observed only for Ce-containing samples, becoming more pronounced with the increase of Ce content. These peaks indicate the formation of NiO-$CeO_2$ solid solutions and represent for the reducible oxygen species absorbed to their oxygen vacancies [15], which is beneficial to the catalytic $NH_3$ decomposition [13,36]. In comparison with the 10Ni/$Al_2O_3$ catalyst, the 10Ni/$Al_1Ce_{0.01}O_x$ shows a shift of the major reduction peak to higher temperature region in the $H_2$-TPR profile, along with its lowest $H_2$ consumption recorded in the range of 40–600 °C (Table 2), indicating that a small amount of Ce addition (Ce/Al = 0.01) can decrease the reducibility of the catalyst. Therefore, the better performance of the 10Ni/$Al_1Ce_{0.01}O_x$ compared to the Ni/$Al_2O_3$ catalyst might have resulted from the synergistic effects of higher Ni dispersion, larger Ni surface area, stronger interaction between Ni and support, and the presence of surface oxygen vacancies in the structure. On the other hand, among the Ce-containing catalysts, the major reduction peak shifted to a lower temperature region (Fig. 6b), and higher $H_2$ consumption was observed with the increase of the Ce/Al molar ratio (Table 2 and S3). Notably, the 10Ni/$Al_1Ce_{0.10}O_x$ catalyst showed a reduction peak in the high-temperature region (855 °C), which is related to the reduction of bulk $CeO_2$ [15]. These observations suggest that higher Ce addition could produce more surface oxygen vacancies due to the formation of more Ni-$CeO_2$ solid solutions. As a result, the catalytic performance increased with Ce addition (Ce/Al up to 0.05) even though Ni dispersion and Ni surface area decreased with the increases of Ce content (Table 2). However, the excessive formation of NiO-$CeO_2$ solid solutions in the high Ce-containing catalyst can decrease reducible NiO species because of the difficulty of reducing $Ni^{2+}$ in this structure, resulting in a negative effect on the catalytic activity [15,37]. Consequently, the $NH_3$ conversion decreased with excessive loading of Ce (Ce/Al = 0.10). In general, what this means is that besides Ni dispersion and Ni surface area, the degree of interaction between Ni and support, and the number of surface oxygen vacancies are also very important in determining the performance of catalysts in this reaction.

Bearing in mind the previous points, XPS analysis of the 10Ni/$Al_1Ce_aO_x$ catalysts was also investigated (Fig. 8). The Ni 2p spectra of these reduced catalysts showed that the peak representing for $Ni^0$ became smaller for the samples with higher Ce loading (Fig. 8a), suggesting that the presence of Ce can decline the reduction of $Ni^{2+}$ to $Ni^0$, and thus the lower surface $Ni^0$ fraction can be obtained (Table 2). Despite having lower surface $Ni^0$ fraction, the catalytic activity keeps increasing with the increase of Ce loading (Ce/Al up to 0.05). However, the decrease in $NH_3$ conversion over the 10Ni/$Al_1Ce_{0.10}O_x$ catalyst could be explained by the very low surface $Ni^0$ fraction after reduction (4.92%), which is consistent with the low Ni dispersion (5.41%) and small Ni surface area (3.90 $m^2$/g) of this sample, as presented in Table 2. On the other hand, the surface $Ce^{3+}$ fraction was increased with the increase of Ce/Al molar ratio from 0.01 to 0.05, then decreased with an extra loading of Ce (Fig. 8b and Table 2). These results reveal that the addition of an appropriate amount of Ce can provide a proper number of oxygen vacancies in the catalyst. Besides this, the $CO_2$ desorption profiles recorded for the 10Ni/$Al_2O_3$ and 10Ni/$Al_1Ce_{0.05}O_x$ catalysts (Fig. S8) indicate that the basicity of catalyst increases with the presence of Ce. The stronger basic nature of the Ce-containing catalyst might have a beneficial effect on the re-combinative desorption of nitrogen atoms due to the electron donation effect of Ce, and thus promotes $NH_3$ decomposition effectively [38,39]. Furthermore, another factor contributing to the better catalytic performance of Ce-containing catalysts than Ni/$Al_2O_3$ could be the smaller Ni size, which was confirmed by TEM observation (Fig. 1 and S3).

To sum up, the presence of Ce can significantly alter the physicochemical properties of the derived catalysts, which can improve the formation of surface oxygen vacancies and the basicity of the catalyst. A small amount of Ce addition can enhance the Ni dispersion, Ni surface area, and Ni-support interaction, but higher Ce addition will oppositely change these parameters. In general, Ce addition is beneficial for the derived catalyst in this reaction, and the optimum amount of Ce addition

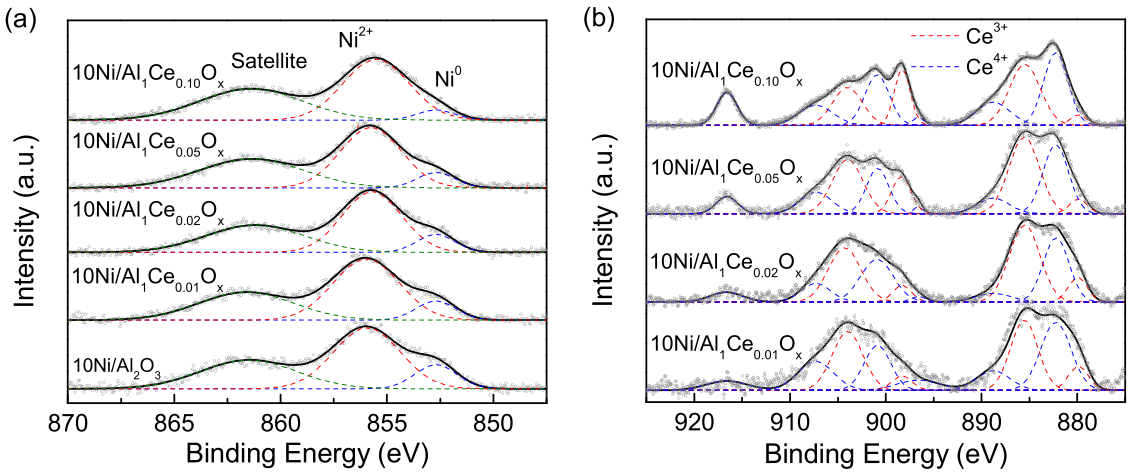


**Fig. 8.** XPS Ni 2p (a) and Ce 3d (b) spectra of the reduced catalysts with different molar ratios of Ce/Al.

should be noted to maximize the catalytic performance.

### 3.4. Possible reaction mechanism

Catalytic $NH_3$ decomposition generally proceeds in a stepwise dehydrogenation of $NH_3$ to produce surface N and H atoms, followed by the recombinative desorption of N and H atoms from the catalyst surface [39,40]. Research has shown that there is as yet no general and straightforward statement of which one is the rate-determining step (RDS) of the reaction, but that such a determination depends on the specific catalyst and reaction conditions [7]. In this work, along with the $NH_3$-TPD-MS and $NH_3$-TPSR-MS analyses, in-situ DRIFTs study of $NH_3$ adsorption was performed to have an insightful understanding of the reaction characteristics at the surface of the catalysts. FTIR spectra of species adsorbed on catalysts due to contact with $NH_3$ at different temperatures are presented in Fig. 9. The FTIR spectral characteristics observed for the $10Ni/Al_2O_3$ and $10Ni/Al_1Ce_{0.05}O_x$ catalysts were relatively identical, suggesting a similar reaction mechanism proceeding over these catalysts. Particularly, after contact with $NH_3$ at 50 °C, the bands observed at around 1680 $cm^{-1}$ and 1475 $cm^{-1}$ were due to the asymmetric and symmetric deformation modes, respectively, of $NH_3$ coordinated on Brønsted acid sites. Whereas, the bands at around 1620 $cm^{-1}$ and 1260 $cm^{-1}$ were assigned to the asymmetric and symmetric deformation modes, respectively, of $NH_3$ coordinated on Lewis acid sites [41,42]. The bands at around 3400 – 3200 $cm^{-1}$ correspond to -NH stretching of adsorbed $NH_3$ [43,44], which are associated with Lewis acid sites. As the temperatures increased, the intensities of these bands gradually decreased or disappeared. These observations can be explained by the desorption of unreacted $NH_3$ and the dehydrogenation of $NH_3$, and have been confirmed by the $NH_3$-TPD-MS results (Fig. 5b and S9b). Besides this, new absorption bands were visible at around 1510, 1456, 1345, 1310, 1154, and 1098 $cm^{-1}$ at temperatures of 200 °C or higher. The bands at around 1510, 1345, 1310, 1154, and 1098 $cm^{-1}$ were assigned to amide ($-NH_2$) scissoring or wagging [44,45]. The band at around 1456 $cm^{-1}$ was ascribed to –NH deformation modes. These results indicate that the adsorbed $NH_3$ was dissociated into $–NH_2$ and –NH intermediates through dehydrogenation at elevated temperatures.

Regarding the RDS of this reaction, as can be seen from the obtained in-situ DRIFT spectra of the catalysts (Fig. 9), the –NH and $–NH_2$ groups can be detected below 300 °C, suggesting that the first dehydrogenation steps could be easily started and proceeded at low reaction temperatures, and thus those steps could not be the RDS of this reaction. This result is in agreement with the computational study of the $NH_3$ decomposition over Ni-based catalysts [27,46]. Therefore, the RDS of the $NH_3$ decomposition reaction over these catalysts could be the recombinative desorption of H and/or N atoms. It should be further noted that, in the $NH_3$-TPD-MS profiles of the catalysts (Fig. 5b and S9b), the main $N_2$ desorption peaks of both catalysts appeared at identical temperature (375 °C). However, the $H_2$ desorption peak of $10Ni/Al_2O_3$ catalyst completed at a higher temperature (385 °C) compared to that of $10Ni/Al_1Ce_{0.05}O_x$ catalyst (360 °C), indicating that the desorption of $H_2$ over the $10Ni/Al_1Ce_{0.05}O_x$ catalyst could proceed more readily. This difference could be resulted from the presence of Ce in the $10Ni/Al_1Ce_{0.05}O_x$ catalyst, which promoted the recombinative desorption of H

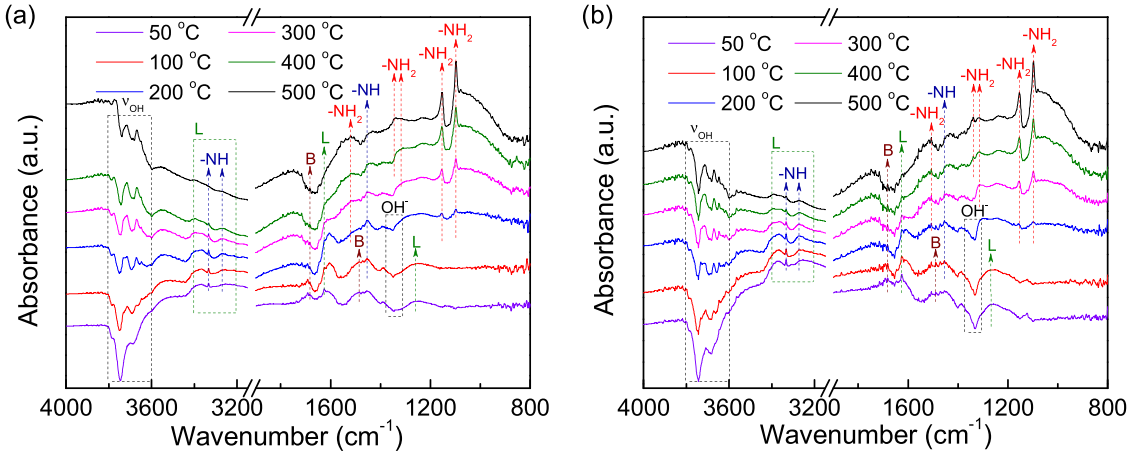


**Fig. 9.** In-situ DRIFTS study of $NH_3$ contacting with the $10Ni/Al_2O_3$ (a) and $10Ni/Al_1Ce_{0.05}O_x$ (b) catalysts during the heating process.

atoms by alleviating adsorption energy due to the stronger basic property [39].

### 3.5. Effect of Ni loading, catalyst synthesis and operating conditions

The catalyst with a Ce/Al molar ratio of 0.05 exhibited the highest activity and thus was selected for further investigation of the effects of Ni loading, calcination conditions, reduction temperature, WHSV, and stability of the catalyst. The catalytic activity of $Ni/Al_1Ce_{0.05}O_x$ catalysts with different Ni contents is shown in Fig. 10a. The $NH_3$ conversion gradually increases with the increase of Ni content from 10 wt% to 40 wt% and then decreases with further increases of Ni loading (60 wt %). This observation is in line with the Ni dispersion, Ni surface area, and surface $Ce^{3+}$ ratio (Table 2), and the highest values of 7.97%, 20.39 $m^2/g$, and 71.00%, respectively, were recorded for the sample contained 40 wt% Ni. The reduction behaviors of these catalysts are shown in Fig. S10; $H_2$ consumption values, observed in the range of 40 – 600 °C are presented in Table 2. Although the $H_2$ consumption kept

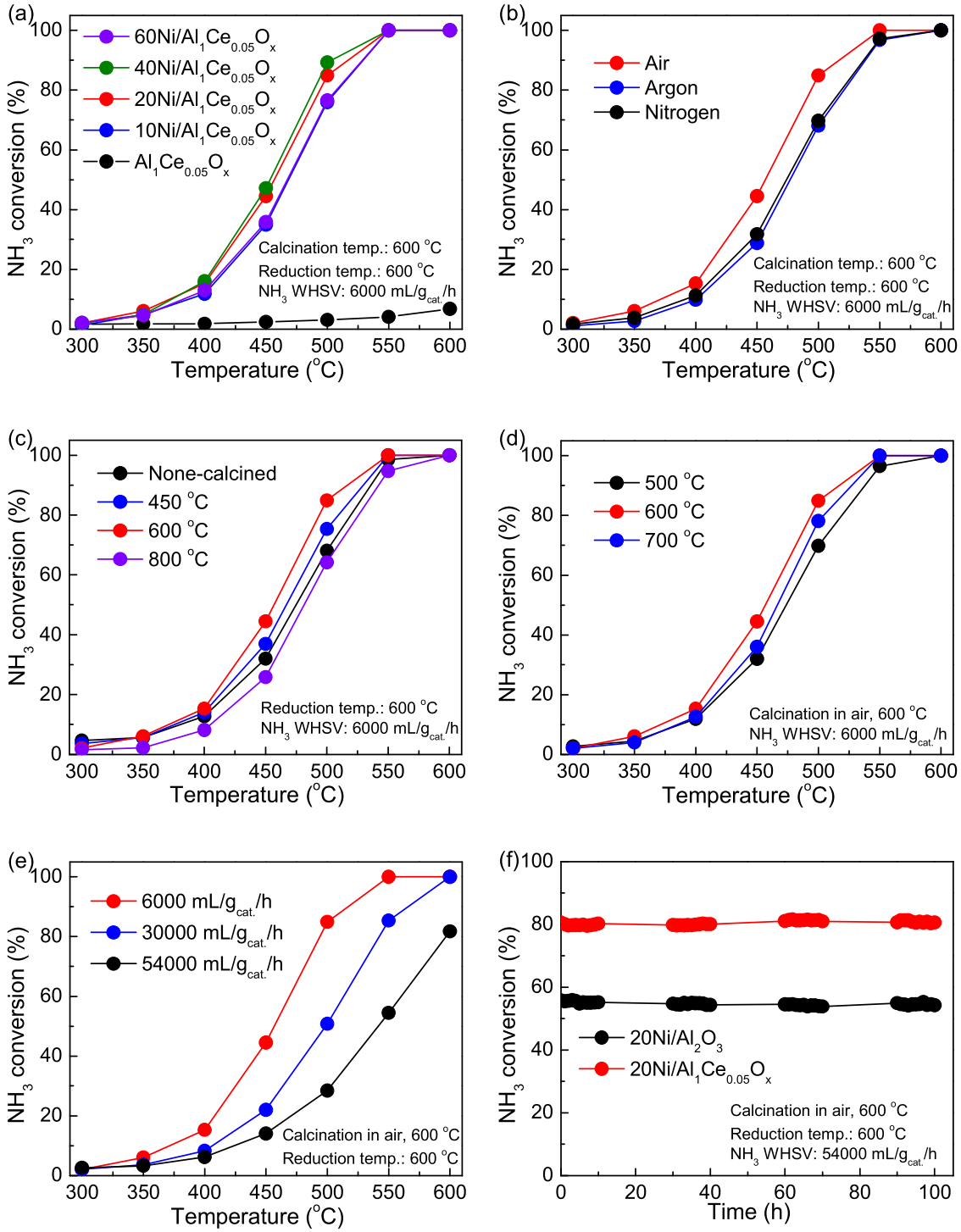


**Fig. 10.** Catalytic activity for $NH_3$ decomposition over $Ni/Al_1Ce_{0.05}O_x$ catalysts with different Ni contents (a); effects of calcination atmosphere (b), calcination temperature (c), reduction temperature (d), and $NH_3$ WHSV (e) on the performance of $20Ni/Al_1Ce_{0.05}O_x$ catalyst; and stability tests on the $20Ni/Al_2O_3$ and $20Ni/Al_1Ce_{0.05}O_x$ catalyst (f).

increasing at higher Ni loading (60 wt%), the Ni dispersion and Ni surface area decreased. This phenomenon could be explained by the increase of NiO particle size at high Ni loading [38], making it harder to be reduced, which can be confirmed by the shifting of the reduction peak to a higher temperature region (Fig. S10), as well as by the calculated surface metallic Ni fraction (Table 2). Based on these results, the highest activity of the catalyst with 40 wt% Ni loading ($40Ni/Al_1Ce_{0.05}O_x$) can mainly be attributed to the association between Ni surface area and the number of surface oxygen vacancies. Though the highest $NH_3$ conversion was obtained with 40 wt% Ni loading, this catalyst did not show much improvement compared to the catalysts containing 20 wt% Ni (Fig. 10a). Hence, Ni loading of 20 wt% was selected to further investigate the effects of catalyst synthesis and operating conditions.

The effects of calcination medium, calcination temperature, reduction temperature, and $NH_3$ WHSV on the catalytic performance of the $20Ni/Al_1Ce_{0.05}O_x$ catalysts are presented in Fig. 10b, c, d, and e. The catalyst calcined in the air atmosphere exhibited better $NH_3$ decomposition activity than did the other catalysts calcined in the nitrogen or argon atmosphere (Fig. 10b). The calcination temperature was examined up to 800 °C in the air atmosphere, and the best catalytic performance was observed for the catalyst calcined at 600 °C (Fig. 10c). The effect of reduction temperature was evaluated at 500 °C - 700 °C, and the optimum reduction temperature was found to be 600 °C (Fig. 10d). Fig. 10e shows the influence of $NH_3$ WHSV on $NH_3$ conversion, which gradually decreased as WHSV increased from 6000 $mL/g_{cat.}/h$ to 54000 $mL/g_{cat.}/h$. To have an insightful understanding of how these parameters affect the catalytic behaviors of the catalysts, further comprehensive study on their characterization is needed.

To evaluate the long-term stability of the catalysts prepared by the CADH method (i.e., $20Ni/Al_2O_3$, $20Ni/Al_1Ce_{0.05}O_x$), experiments were carried out at 600 °C for 100 h with a WHSV of 54000 $mL/g_{cat.}/h$; the results are shown in Fig. 10f. $NH_3$ conversions over $20Ni/Al_2O_3$ and $20Ni/Al_1Ce_{0.05}O_x$ were stably maintained at around 80.0% and 55.0%, respectively, without any obvious decrease during 100 h operation. Such exceptional catalytic stability of the prepared catalysts makes them very promising candidates for practical application in this field. Besides this, Table 3 shows a comparison of the catalytic performance at 500 °C of the prepared catalysts with various catalysts reported in the current literature. Noticeably, the catalysts proposed in this study demonstrate outstanding catalytic capability for $NH_3$ decomposition compared to other Ni-based catalysts and are even comparable with some Ru-based catalysts. These findings suggest the applicability of the one-pot CADH synthetic method and its derived materials can serve as competent catalysts in $NH_3$ decomposition for hydrogen generation.

## 4. Conclusion

This paper presented a series of $Ni/Al_1Ce_{0.05}O_x$ catalysts prepared by the one-pot CADH, CADH-WI, CP, and CP-WI methods; it also looks at the promotional effects of Ce on the physicochemical properties and catalytic performance of catalysts prepared by the one-pot CADH method, and optimization of the $NH_3$ decomposition reaction. The one-pot CADH method can provide the catalyst with higher Ni dispersion and surface area, superior Ni reducibility, more surface oxygen vacancy, and better $NH_3$ adsorption affinity, yielding the best catalytic activity with the lowest apparent activation energy, and making this a promising approach for the preparation of non-noble metal catalysts applied in this field. $NH_3$ conversion over $20Ni/Al_1Ce_{0.05}O_x$ catalyst at 600 °C and WHSV of 54000 $mL/g_{cat.}/h$ can be reached at 81.8% with an $H_2$ formation rate of 49.3 $mmol/g_{cat.}/min$, and that performance can be stably maintained for 100 h continuous operation. The appropriate amount of Ce addition can harmonize the synergistic effects of NiO reducibility, surface oxygen vacancies, basicity, and Ni-support interaction in the derived catalyst, thus maximizing the catalytic performance for decomposition of $NH_3$. This work could propose one of the most promising non-noble metal-based catalysts for $NH_3$ decomposition, and facilitate the use of $NH_3$ in the hydrogen economy.

## CRediT authorship contribution statement

**Quoc Cuong Do:** Investigation, Methodology, Formal analysis, Writing – original draft. **Youngmin Kim:** Validation, Visualization, Writing – review & editing. **Thien An Le:** Investigation, Writing – review & editing. **Geo Jong Kim:** Formal analysis, Writing – review & editing. **Jeong-Rang Kim:** Validation, Writing – review & editing. **Tae-Wan Kim:** Validation, Writing – review & editing. **You-Jin Lee:** Formal analysis. **Ho-Jeong Chae:** Conceptualization, Supervision, Funding acquisition, Project administration, Resources.

## Declaration of Competing Interest

The authors declare that they have no known competing financial

**Table 3**
Comparison of the catalytic performance of the prepared catalysts with various reported Ni-based and Ru-based catalysts for $NH_3$ decompositions at 500 °C.

| Catalysts | Ni or Ru (wt%) | $NH_3$ WHSV ($mL/g_{cat.}/h$) | $X_{NH_3}$ (%) | $r_{H_2}$ ($mmol/g_{cat.}/min$) | $E_{app}$ (kJ/mol)[a] | [Ref.], Year |
|---|---|---|---|---|---|---|
| $10Ni/Al_2O_3$ | 9.6 | 6000 | 43.0 | 2.9 | 84.2 | This work |
| $10Ni/Al_1Ce_{0.05}O_x$ | 9.6 | 6000 | 76.0 | 5.1 | 74.7 | |
| $20Ni/Al_1Ce_{0.05}O_x$ | 19.3 | 6000 | 84.9 | 5.7 | – | |
| | | 30000 | 50.8 | 17.0 | 70.8 | |
| | | 54000 | 28.4 | 17.2 | – | |
| Ni/CaNH-HS | 10 | 30000 | 58.6 | 19.6 | – | [47], 2021 |
| Ni/CaNH | | | 38.3 | 12.8 | – | |
| Ni/Ba-Al-O | 20 | 6000 | 54.1 | 3.6 | 76.5 | [39], 2020 |
| $Ni/Al_2O_3$ | 8.9 | 9000 | 27.0 | 2.7 | 91.5 | [48], 2020 |
| $Ni/Ce_{0.8}Zr_{0.2}O_2$ | 10.7 | | 48.0 | 4.8 | 73.8 | |
| $Ni/Al\text{-}Ce_{0.8}Zr_{0.2}O_2$ | 8.0 | | 58.0 | 5.9 | 66.8 | |
| $Ni_1$/C-LDHs-ST | 23.6 | 30000 | 20.0 | 6.7 | – | [49], 2020 |
| Ni/ZSM-5 | 5 | 30000 | 42.0 | 14.1 | 88.1 | [50], 2018 |
| $Ni\text{-}30/ATP@SiO_2$ | 8.7 | 30000 | 16.0 | 5.4 | 80.1 | [51], 2016 |
| Ni/MWCNT | 5 | 6000 | 57.6 | 3.9 | – | [52], 2014 |
| $Ni\text{-}La/Al_2O_3$ | 37.9 | 30000 | 71.9 | 24.1 | – | [15], 2008 |
| $Ni\text{-}Ce/Al_2O_3$ | 43.4 | 30000 | 63.9 | 21.4 | – | [53], 2005 |
| Ru/Rb-Y | 2.0 | 30000 | 51.0 | 17.1 | 78.5 | [54], 2021 |
| Ru/red mud | 5.5 | 30000 | 27.0 | 9.6 | – | [55], 2020 |
| $Ru/Al_2O_3$ | 2.1 | 30000 | 21.0 | 7.0 | 121.7 | [56], 2019 |
| Ru/CNTs | 2.5 | | 41.0 | 13.7 | 86.5 | |
| $Ru/Ba\text{-}ZrO_2$ | 3.0 | 30000 | 53.0 | 17.8 | 94.1 | [57], 2019 |

[a] Apparent activation energy that calculated using the Arrhenius equation.

interests or personal relationships that could have appeared to influence the work reported in this paper.

## Acknowledgments

This work was supported by the core KRICT project (SI2111–30) from the Korea Research Institute of Chemical Technology (KRICT) and by the Korea Institute of Energy Technology Evaluation and Planning (KETEP) (No. 20213030040550) and by the Alchemist Project (No. 20012383) from the Ministry of Trade, Industry & Energy (MOTIE) of the Republic of Korea.

## Appendix A. Supporting information

Supplementary data associated with this article can be found in the online version at doi:10.1016/j.apcatb.2022.121167.

## References

[1] Y. Gu, Y. Ma, Z. Long, S. Zhao, Y. Wang, W. Zhang, One-pot synthesis of supported Ni@$Al_2O_3$ catalysts with uniform small-sized Ni for hydrogen generation via ammonia decomposition, Int. J. Hydrog. Energy 46 (2021) 4045–4054.
[2] A.K. Singh, S. Singh, A. Kumar, Hydrogen energy future with formic acid: a renewable chemical hydrogen storage system, Catal. Sci. Technol. 6 (2016) 12–40.
[3] K. Nagaoka, T. Eboshi, Y. Takeishi, R. Tasaki, K. Honda, K. Imamura, K. Sato, Carbon-free $H_2$ production from ammonia triggered at room temperature with an acidic $RuO_2$/γ-$Al_2O_3$ catalyst, Sci. Adv. 3 (2017), e1602747.
[4] K. Okura, K. Miyazaki, H. Muroyama, T. Matsui, K. Eguchi, Ammonia decomposition over Ni catalysts supported on perovskite-type oxides for the on-site generation of hydrogen, RSC Adv. 8 (2018) 32102–32110.
[5] J. Guo, P. Chen, Catalyst: $NH_3$ as an Energy Carrier, Chem 3 (2017) 709–712.
[6] T.E. Bell, L. Torrente-Murciano, $H_2$ Production via Ammonia Decomposition Using Non-Noble Metal Catalysts: A Review, Top. Catal. 59 (2016) 1438–1457.
[7] T.A. Le, Q.C. Do, Y.M. Kim, T.W. Kim, H.J. Chae, A review on the recent developments of ruthenium and nickel catalysts for $CO_x$-free $H_2$ generation by ammonia decomposition, Korean J. Chem. Eng. 38 (2021) 1087–1103.
[8] J.C. Ganley, F.S. Thomas, E.G. Seebauer, R.I. Masel, A Priori Catalytic Activity Correlations: The Difficult Case of Hydrogen Production from Ammonia, Catal. Lett. 96 (2004) 117–122.
[9] K. Okura, T. Okanishi, H. Muroyama, T. Matsui, K. Eguchi, Promotion effect of rare-earth elements on the catalytic decomposition of ammonia over Ni/$Al_2O_3$ catalyst, Appl. Catal. A 505 (2015) 77–85.
[10] H. Muroyama, C. Saburi, T. Matsui, K. Eguchi, Ammonia decomposition over Ni/$La_2O_3$ catalyst for on-site generation of hydrogen, Appl. Catal. A 443–444 (2012) 119–124.
[11] I. Nakamura, T. Fujitani, Role of metal oxide supports in $NH_3$ decomposition over Ni catalysts, Appl. Catal. A 524 (2016) 45–49.
[12] K.R.B. Singh, V. Nayak, T. Sarkar, R.P. Singh, Cerium oxide nanoparticles: properties, biosynthesis and biomedical application, RSC Adv. 10 (2020) 27194–27214.
[13] T.A. Le, Y. Kim, H.W. Kim, S.-U. Lee, J.-R. Kim, T.-W. Kim, Y.-J. Lee, H.-J. Chae, Ru-supported lanthania-ceria composite as an efficient catalyst for $CO_x$-free $H_2$ production from ammonia decomposition, Appl. Catal. B 285 (2021), 119831.
[14] N. Morlanés, S. Sayas, G. Shterk, S.P. Katikaneni, A. Harale, B. Solami, J. Gascon, Development of a Ba–CoCe catalyst for the efficient and stable decomposition of ammonia, Catal. Sci. Technol. 11 (2021) 3014–3024.
[15] W. Zheng, J. Zhang, Q. Ge, H. Xu, W. Li, Effects of $CeO_2$ addition on Ni/$Al_2O_3$ catalysts for the reaction of ammonia decomposition to hydrogen, Appl. Catal. B 80 (2008) 98–105.
[16] P. Vacharapong, S. Arayawate, S. Henpraserttae, S. Katanyutanon, S. Charojrochkul, L. Lawtrakul, P. Toochinda, Effect of Magnetic Inducement in Preparation of Ni/Ce-doped $Al_2O_3$ for Ammonia Decomposition, ChemistrySelect 4 (2019) 11913–11919.
[17] D. Beierlein, D. Häussermann, M. Pfeifer, T. Schwarz, K. Stöwe, Y. Traa, E. Klemm, Is the $CO_2$ methanation on highly loaded Ni-$Al_2O_3$ catalysts really structure-sensitive? Appl. Catal. B 247 (2019) 200–219.
[18] Y.-S. Jung, W.-L. Yoon, Y.-S. Seo, Y.-W. Rhee, The effect of precipitants on Ni-$Al_2O_3$ catalysts prepared by a co-precipitation method for internal reforming in molten carbonate fuel cells, Catal. Commun. 26 (2012) 103–111.
[19] A. Zhao, W. Ying, H. Zhang, H. Ma, D. Fang, Ni–$Al_2O_3$ catalysts prepared by solution combustion method for syngas methanation, Catal. Commun. 17 (2012) 34–38.
[20] P. Jiang, J. Zhao, Y. Han, X. Wang, Y. Pei, Z. Zhang, Y. Liu, J. Ren, Highly Active and Dispersed Ni/$Al_2O_3$ Catalysts for CO Methanation Prepared by the Cation–Anion Double-Hydrolysis Method: Effects of Zr, Fe, and Ce Promoters, Ind. Eng. Chem. Res. 58 (2019) 11728–11738.
[21] P. Bai, W. Xing, Z. Zhang, Z. Yan, Facile synthesis of thermally stable mesoporous crystalline alumina by using a novel cation–anion double hydrolysis method, Mater. Lett. 59 (2005) 3128–3131.
[22] P. Bai, P. Wu, Z. Yan, X.S. Zhao, Cation–anion double hydrolysis derived mesoporous γ-$Al_2O_3$ as an environmentally friendly and efficient aldol reaction catalyst, J. Mater. Chem. 19 (2009) 1554–1563.
[23] K. Kishida, M. Kitano, M. Sasase, P.V. Sushko, H. Abe, Y. Niwa, K. Ogasawara, T. Yokoyama, H. Hosono, Air-Stable Calcium Cyanamide-Supported Ruthenium Catalyst for Ammonia Synthesis and Decomposition, ACS Appl. Energy Mater. 3 (2020) 6573–6582.
[24] X. Meng, C. Wan, Y. Wang, X. Ju, Porous Ni@C derived from bimetallic Metal–Organic Frameworks and its application for improving $LiBH_4$ dehydrogenation, J. Alloy. Compd. 735 (2018) 1637–1647.
[25] L. Barrio, A. Kubacka, G. Zhou, M. Estrella, A. Martínez-Arias, J.C. Hanson, M. Fernández-García, J.A. Rodriguez, Unusual Physical and Chemical Properties of Ni in $Ce_{1-x}Ni_xO_{2-y}$ Oxides: Structural Characterization and Catalytic Activity for the Water Gas Shift Reaction, J. Phys. Chem. C. 114 (2010) 12689–12697.
[26] Y. Qiu, E. Fu, F. Gong, R. Xiao, Catalyst support effect on ammonia decomposition over Ni/$MgAl_2O_4$ towards hydrogen production, Int. J. Hydrog. Energy 47 (2022) 5044–5052.
[27] X. Duan, G. Qian, C. Fan, Y. Zhu, X. Zhou, D. Chen, W. Yuan, First-principles calculations of ammonia decomposition on Ni(110) surface, Surf. Sci. 606 (2012) 549–553.
[28] A.P. Grosvenor, M.C. Biesinger, R.S.C. Smart, N.S. McIntyre, New interpretations of XPS spectra of nickel metal and oxides, Surf. Sci. 600 (2006) 1771–1779.
[29] K. Kamonsuangkasem, S. Therdthianwong, A. Therdthianwong, N. Thammajak, Remarkable activity and stability of Ni catalyst supported on $CeO_2$-$Al_2O_3$ via $CeAlO_3$ perovskite towards glycerol steam reforming for hydrogen production, Appl. Catal. B 218 (2017) 650–663.
[30] C. Jiang, E. Loisel, D.A. Cullen, J.A. Dorman, K.M. Dooley, On the enhanced sulfur and coking tolerance of Ni-Co-rare earth oxide catalysts for the dry reforming of methane, J., Catal. 393 (2021) 215–229.
[31] E. Yang, E. Nam, J. Lee, H. Lee, E.D. Park, H. Lim, K. An, $Al_2O_3$-Coated Ni/$CeO_2$ nanoparticles as coke-resistant catalyst for dry reforming of methane, Catal. Sci. Technol. 10 (2020) 8283–8294.
[32] M.E. Khan, M.M. Khan, M.H. Cho, $Ce^{3+}$-ion, Surface Oxygen Vacancy, and Visible Light-induced Photocatalytic Dye Degradation and Photocapacitive Performance of $CeO_2$-Graphene Nanostructures, Sci. Rep. 7 (2017) 5928.
[33] S. Zhang, W. Cai, J. Yu, C. Ji, N. Zhao, A facile one-pot cation-anion double hydrolysis approach to the synthesis of supported MgO/γ-$Al_2O_3$ with enhanced adsorption performance towards $CO_2$, Chem. Eng. J. 310 (2017) 216–225.
[34] G. Li, M. Kanezashi, T. Tsuru, Highly enhanced ammonia decomposition in a bimodal catalytic membrane reactor for $CO_x$-free hydrogen production, Catal. Commun. 15 (2011) 60–63.
[35] H. Liu, X. Zou, X. Wang, X. Lu, W. Ding, Effect of $CeO_2$ addition on Ni/$Al_2O_3$ catalysts for methanation of carbon dioxide with hydrogen, J. Nat. Gas. Chem. 21 (2012) 703–707.
[36] C. Huang, Y. Yu, X. Tang, Z. Liu, J. Zhang, C. Ye, Y. Ye, R. Zhang, Hydrogen generation by ammonia decomposition over Co/$CeO_2$ catalyst: Influence of support morphologies, Appl. Surf. Sci. 532 (2020), 147335.
[37] G. Wrobel, M.P. Sohier, A. D'Huysser, J.P. Bonnelle, J.P. Marcq, Hydrogenation catalysts based on nickel and rare earth oxides: Part II: XRD, electron microscopy and XPS studies of the cerium-nickel-oxygen-hydrogen system, Appl. Catal. A 101 (1993) 73–93.
[38] K. Okura, T. Okanishi, H. Muroyama, T. Matsui, K. Eguchi, Ammonia Decomposition over Nickel Catalysts Supported on Rare-Earth Oxides for the On-Site Generation of Hydrogen, ChemCatChem 8 (2016) 2988–2995.
[39] Y. Im, H. Muroyama, T. Matsui, K. Eguchi, Ammonia decomposition over nickel catalysts supported on alkaline earth metal aluminate for $H_2$ production, Int. J. Hydrog. Energy 45 (2020) 26979–26988.
[40] J. Zhao, C. Cui, H. Wang, J. Han, X. Zhu, Q. Ge, Insights into the Mechanism of Ammonia Decomposition on Molybdenum Nitrides Based on DFT Studies, J. Phys. Chem. C. 123 (2019) 554–564.
[41] M. Amblard, R. Burch, B.W.L. Southward, A study of the mechanism of selective conversion of ammonia to nitrogen on Ni/γ-$Al_2O_3$ under strongly oxidising conditions, Catal. Today 59 (2000) 365–371.
[42] L. Zhang, H. He, Mechanism of selective catalytic oxidation of ammonia to nitrogen over Ag/$Al_2O_3$, J., Catal. 268 (2009) 18–25.
[43] M.A. Larrubia, G. Ramis, G. Busca, An FT-IR study of the adsorption and oxidation of N-containing compounds over $Fe_2O_3$-$TiO_2$ SCR catalysts, Appl. Catal. B 30 (2001) 101–110.
[44] S. He, C. Zhang, M. Yang, Y. Zhang, W. Xu, N. Cao, H. He, Selective catalytic oxidation of ammonia from MAP decomposition, Sep. Purif. Technol. 58 (2007) 173–178.
[45] W.S. Kijlstra, D.S. Brands, E.K. Poels, A. Bliek, Mechanism of the Selective Catalytic Reduction of NO by $NH_3$ over $MnO_x$/$Al_2O_3$, J. Catal. 171 (1997) 208–218.
[46] X. Duan, G. Qian, Y. Liu, J. Ji, X. Zhou, D. Chen, W. Yuan, Structure sensitivity of ammonia decomposition over Ni catalysts: A computational and experimental study, Fuel Process. Technol. 108 (2013) 112–117.
[47] K. Ogasawara, T. Nakao, K. Kishida, T.-N. Ye, Y. Lu, H. Abe, Y. Niwa, M. Sasase, M. Kitano, H. Hosono, Ammonia Decomposition over CaNH-Supported Ni Catalysts via an $NH_2$–-Vacancy-Mediated Mars–van Krevelen Mechanism, ACS Catal. 11 (2021) 11005–11015.
[48] D. Sima, H. Wu, K. Tian, S. Xie, J.J. Foo, S. Li, D. Wang, Y. Ye, Z. Zheng, Y.-Q. Liu, Enhanced low temperature catalytic activity of Ni/Al–$Ce_{0.8}Zr_{0.2}O_2$ for hydrogen production from ammonia decomposition, Int. J. Hydrog. Energy 45 (2020) 9342–9352.

[49] J. Zhao, L. Deng, W. Zheng, S. Xu, Q. Yu, X. Qiu, Nickel-induced structure transformation in hydrocalumite for enhanced ammonia decomposition, Int. J. Hydrog. Energy 45 (2020) 12244–12255.
[50] Z.-P. Hu, C.-C. Weng, C. Chen, Z.-Y. Yuan, Catalytic decomposition of ammonia to $CO_x$-free hydrogen over Ni/ZSM-5 catalysts: A comparative study of the preparation methods, Appl. Catal. A 562 (2018) 49–57.
[51] L. Li, F. Chen, J. Shao, Y. Dai, J. Ding, Z. Tang, Attapulgite clay supported Ni nanoparticles encapsulated by porous silica: Thermally stable catalysts for ammonia decomposition to $CO_x$ free hydrogen, Int. J. Hydrog. Energy 41 (2016) 21157–21165.
[52] H. Zhang, Y.A. Alhamed, Y. Kojima, A.A. Al-Zahrani, H. Miyaoka, L.A. Petrov, Structure and catalytic properties of Ni/MWCNTs and Ni/AC catalysts for hydrogen production via ammonia decomposition, Int. J. Hydrog. Energy 39 (2014) 277–287.
[53] J. Zhang, H. Xu, X. Jin, Q. Ge, W. Li, Characterizations and activities of the nano-sized $Ni/Al_2O_3$ and $Ni/La–Al_2O_3$ catalysts for $NH_3$ decomposition, Appl. Catal. A 290 (2005) 87–96.
[54] J. Cha, T. Lee, Y.-J. Lee, H. Jeong, Y.S. Jo, Y. Kim, S.W. Nam, J. Han, K.B. Lee, C. W. Yoon, H. Sohn, Highly monodisperse sub-nanometer and nanometer Ru particles confined in alkali-exchanged zeolite Y for ammonia decomposition, Appl. Catal. B 283 (2021), 119627.
[55] S.F. Kurtoğlu, S. Soyer-Uzun, A. Uzun, Utilizing red mud modified by simple treatments as a support to disperse ruthenium provides a high and stable performance for $CO_x$-free hydrogen production from ammonia, Catal. Today 357 (2020) 425–435.
[56] Z. Wang, Z. Cai, Z. Wei, Highly Active Ruthenium Catalyst Supported on Barium Hexaaluminate for Ammonia Decomposition to $CO_x$-Free Hydrogen, ACS Sustain. Chem. Eng. 7 (2019) 8226–8235.
[57] Z. Wang, Y. Qu, X. Shen, Z. Cai, Ruthenium catalyst supported on Ba modified $ZrO_2$ for ammonia decomposition to $CO_x$-free hydrogen, Int. J. Hydrog. Energy 44 (2019) 7300–7307.